



ISSN: 0067-2904

MHD Flow of Jeffery Nanofluid Through Symmetric Ciliated Channel with Porous Medium: Biological Application

Hayat A. Ali^{1*}, Ahmed M. Abdulhadi², Saba S. Hassan¹, Bushra. E.Kashem¹

¹Department of Applied Science, University of Technology-Iraq, Baghdad, Iraq

²Department of Mathematics, College of Science, University of Baghdad, Baghdad, Iraq

Received: 18/9/2022

Accepted: 19/2/2023

Published: 30/4/2024

Abstract

This paper emphasizes on examining the impact of a magnetic field, and porous medium on the non-Newtonian Jeffery nanofluid flows due to metachronal waves induced by ciliated structures that covering the inner walls of the symmetric channel. The governing equations namely continuity, motion, energy and nanoparticles concentration are formulated with suitable boundary conditions and simplified depending on the assumption of long wavelength and low Reynolds number. The simplified equations are solved by using Mathematica program. Further, these analytical solutions for velocity profile, temperature, concentration profiles and streamlines are graphically elucidated and discussed in detail. we concluded that the Hartman number and permeability parameter have opposite effect on the flow characteristics. Moreover, the Jeffery parameter λ_1 has an increasing impact on the velocity profile whereas the dimensionless eccentricity of ellipse parameter α decreases the velocity profile of the fluid.

Keywords: Jeffery fluid, Nanofluid, Ciliated channel, Porous medium.

تدفق MHD لمائع جفري النانوي عبر قناة مهدبة متماثلة ذات وسط مسامي: تطبيق بيولوجي

حياة عادل علي¹, احمد مولود عبدالهادي², صبا ستار حسن¹, بشرى عيسى غشيم¹

قسم العلوم التطبيقية، الجامعة التكنولوجية-العراق، بغداد، العراق

قسم الرياضيات، كلية العلوم، جامعة بغداد، بغداد، العراق

الخلاصة

ركزت هذه الورقة على فحص تأثير المجال المغناطيسي والوسط المسامي على تدفق مائع نانوي لا نيوتيني جفري بسبب موجات متسارعة التي تحدثها الهياكل الهدبية التي تغطي الجدران الداخلية للقناة المتماثلة. تمت صياغة المعادلات الحاكمة (الاستمرارية، والحركة، والطاقة، وتركيز الجسيمات النانوية) بشروط حدودية مناسبة وبسبب اعتمادها على افتراض الطول الموجي الطويل وعدد رينولدز المنخفض، تم حل المعادلات المبسطة باستخدام برنامج ماثماتيكا. علاوة على ذلك، تم توضيح هذه الحلول التحليلية لمف تعريف السرعة ودرجة الحرارة وملامح التركيز والمخططات الانسيابية بيانياً ومناقشتها بالتفصيل. استنتجنا أن رقم هارتمان ومعامل النفاذية لهما تأثير معاكس على خصائص التدفق. علاوة على ذلك، إن معلمة جفري λ_1 لها تأثير متزايد على ملف تعريف السرعة بينما الانحراف اللامركزي لمعلمة القطع الناقص α يقلل من سرعة المائع.

*Email: Hayat.A.Ali@uotechnology.edu.iq

Introduction

Cilia's hair resembles tiny and dense structures, it effects on a huge variety of eukaryotic cells of animal kingdoms. They are naturally fabricated instruments present by a wide biological and physical system to sense or help pass liquids over their surfaces. Cilia motion is essential in many physiological processes such as respiration, locomotion, circulation, reproduction and alimentation [1] [2] [3]. A metachronal wave or an oscillatory motion is formed by the envelope of cilia tips, which in turn assist in transporting the fluid in the ductus such as male sperms in the female cervical canal. However, it is found that the information related the metachronal wave and cilia mechanism is few. Metachronal waves are classified into various types depending on the dynamics and strokes of the cilia motion. If the propagative metachronal waves and the main flow in the same direction, this induces a symplectic beat pattern, whereas antiplectic patterns are generated if they are opposite in their direction. The main attempt has made by Sleigh [4], and Miller [5] who studied the movement of viscous fluid via metachronal waves. After that Khaderi et al. [6] explained the rigorous results related to the metachronal movement of symmetric beating cilia that creates a gradient of pressure in the flow field direction. Recently many efforts in cilia transport of various fluid models achieved. For more detail see [7] [8] [9].

Nanofluid is powerful in many procedures to achieve industrial requirements, like propellant combustion, drug delivery, cooling of automotive engines, and extraction of geothermal forces, and it contains nanometer-sized particles that are called nanoparticles [10]. These fluids are essentially a homogenous mixture of nanoparticles and base fluid. Metals, oxides or nonmetals are types of nanoparticles that are used in nanofluids while the base fluid is usually a conductive fluid, like water or ethylene glycol. The study of nanofluids has gained the attention of numerous researchers because they significantly improve the thermal conductivity of the base fluid, which is beyond the explanation of any existing theory. They are also very stable and have no additional problems, such as sedimentation, erosion, further pressure drop, etc. Choi [11] was the first who presented the nanofluids model. Nowadays, there is a continuous focus of the researchers on the flow analysis of nanofluids. Nowar [12] investigated the peristaltic flow of a nanofluid in a vertical asymmetric channel through a porous medium under the effect of Hall force by using the homotopy perturbation method. The impact of combined convection on heat transfer on pseudoplastic nanofluid flow towards an extendable Riga surface is numerically simulated by Rehman et al. [13]. Aamir Ali et al. [14] examined the combined effects of surface deformation and peristaltic motion of the walls on the nanofluid flow with coupled double diffusion analysis in a channel. Various studies have been illustrated for (Newtonian/non-Newtonian) nanofluid flow through channels with different configurations and effects, see [8] [15].

Motivated by the above literature especially our gap in this study was then extended the investigation that is given by Imran et al. [10] which developed the nanofluids with metachronal rhythm through ductus differences by considering the flow in a ciliated channel to figure out the effect of magnetic field and porous medium. This study has numerous applications in physiology (human male reproductive system) and industry as well. The flow is analyzed for a non-Newtonian Jeffrey nanofluid that is generated by wavy motion via cilia tips. The governing equations are modelled and converted into a system of partial differential equations by employing the long wavelength and low Reynolds number approximations for which the analytical solutions for the problem mathematically are obtained. Finally, the analytical results for the velocity field, temperature distribution, nanoparticles concentration, heat transfer and streamlines are studied in detail with graphs for different key parameters.

Mathematical modeling of the problem

Taking into consideration the unsteady flow of incompressible MHD Jeffery nanofluid under the action of a transverse magnetic field B_0 normal to the flow through a two dimensional symmetric channel filled with porous medium (see Figure 1). The channel is ciliated with a metachronal wave pattern due to the existence of cilia tips which possess along the infinite length in \hat{X} , and \hat{Y} directions where the \hat{X} -axis lies along the centre of the channel and \hat{Y} -axis is transverse to the fluid flow. The flow is induced by the collective beating of the cilia and moves in the \hat{X} direction at a constant wave velocity c along the channel wall.

The mathematical description for the elliptical pattern of the cilia tips envelope is defined as [16].

$$\hat{Y} = F(\hat{X}, \hat{t}) = \pm \hat{H} = d + d\epsilon \cos \left((2\pi\lambda^{-1})(\hat{X} - c\hat{t}) \right) \tag{1}$$

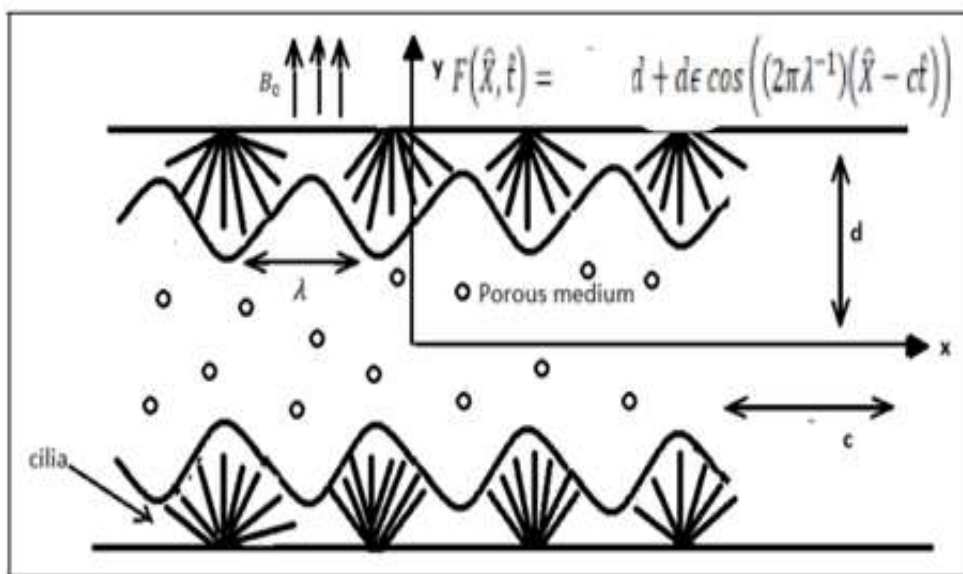


Figure 1: Geometry of ciliated channel [2]

While the horizontal cilia tip is expressed as [1]

$$\hat{X} = G(\hat{X}_0, \hat{X}_0, \hat{t}) = \hat{X}_0 + \alpha \epsilon d \sin \left((2\pi\lambda^{-1})(\hat{X} - c\hat{t}) \right) \tag{2}$$

Where d is the mean half thickness of the channel, ϵ is a dimensionless magnitude of the cilia length, λ is the metachronal wavelength, \hat{X}_0 is the fixed position of the particle, and α is the elliptical motion eccentricity value.

The basic equations for conservation of mass, the momentum of MHD nano-fluid through porous medium, energy, and concentration equations expressed respectively, as follows:

$$\nabla \cdot U = 0, \tag{3}$$

$$\rho_f \frac{d\bar{U}}{d\hat{t}} = -\nabla \bar{P} + \nabla \cdot \bar{S} + J \times B_0 - R + \rho_f g \beta_{\bar{T}} (\bar{T} - T_0) + \rho_f g \beta_{\bar{C}} (\bar{C} - C_0), \tag{4}$$

$$c \rho_f \frac{d\bar{T}}{d\hat{t}} = K \nabla^2 \bar{T} + c \rho_p \left(D_B \nabla \bar{C} \cdot \nabla \bar{T} + \frac{K_T}{T_m} \nabla \bar{T} \cdot \nabla \bar{T} \right), \tag{5}$$

$$\frac{d\bar{C}}{d\hat{t}} = D_B \nabla^2 \bar{C} + \frac{D_T}{T_m} \nabla^2 \bar{T}, \tag{6}$$

Where ρ_f is the fluid density, ρ_p is the particle density, \bar{P} is the pressure term, $U = (\tilde{U}, \tilde{V}, 0)$ is the velocity vector, $(R = \frac{\mu}{\kappa_0} U)$ is the porous medium, K is the thermal conductivity, \bar{T} exhibits fluid temperature field, g the gravitational acceleration, $\beta_{\bar{T}}$ the thermal expansion coefficient, $\beta_{\bar{C}}$ the concentration expansion coefficient, \bar{C} is the nanoparticle field, D_B is the Brownian diffusion coefficient, K_T is the thermal diffusion, T_m is the fluid mean temperature, and D_T denotes the thermophoretic diffusion coefficient.

However, the expression of Cauchy stress tensor \bar{S} for Jeffrey nanofluid is [17].

$$\bar{S} = \frac{\mu}{1+\lambda_1} \left(\dot{\gamma} + \lambda_2 \frac{d\dot{\gamma}}{dt} \right), \tag{7}$$

\bar{S} refers to the extra stress tensor, μ assigns the dynamical viscosity, λ_1 , and λ_2 are the ratios of relaxation to retardation times, $\dot{\gamma}$ is the shear rate and $\frac{d}{dt}$ is the material time differentiation.

Eqs.(1) and (2) can be utilized to evaluate the axial and transverse velocity components of cilia tips as below

$$\begin{aligned} \tilde{U} &= A \frac{\partial \tilde{U}}{\partial \hat{Y}} + \frac{-(2\pi\lambda^{-1})(\alpha d \varepsilon c \cos((2\pi\lambda^{-1})(\hat{X}-c\hat{t}))}{1-(2\pi\lambda^{-1})(\alpha d \varepsilon c \cos((2\pi\lambda^{-1})(\hat{X}-c\hat{t})))}, \\ \tilde{V} &= \frac{(2\pi\lambda^{-1})(d \varepsilon c \sin((2\pi\lambda^{-1})(\hat{X}-c\hat{t}))}{1-(2\pi\lambda^{-1})(\alpha d \varepsilon c \cos((2\pi\lambda^{-1})(\hat{X}-c\hat{t})))}, \text{ at } \hat{Y} = \hat{H} \end{aligned} \tag{8}$$

Defining the following transformation which relates to the fixed $(\hat{X}, \hat{Y}, \hat{t})$ and moving frame (\hat{x}, \hat{y}) as $\hat{X} = \hat{x} + c\hat{t}$, $\hat{Y} = \hat{y}$, $\tilde{U} = \tilde{u} + c$, $\tilde{V} = \tilde{v}$, the unsteady flow transformed into a steady flow which moves with the metachronal wave velocity.

Now, we introduce the following non-dimensional scaling parameters [5] [12].

$$\begin{aligned} x = \frac{\hat{x}}{\lambda}, y = \frac{\hat{y}}{d}, h = \frac{\hat{H}}{d}, \delta = \frac{d}{\lambda}, u = \frac{\tilde{u}}{c}, v = \frac{\tilde{v}}{\delta c}, Re = \frac{cd\rho_f}{\mu}, \theta = \frac{\bar{T}-T_0}{T_1-T_0}, Pr = \frac{\mu c \rho_f}{K}, H^2 = \frac{\sigma B_0^2 d^2}{\mu}, \kappa = \frac{\kappa_0}{d^2}, \omega = \frac{\bar{C}-C_0}{C_1-C_0}, p = \frac{d^2 \bar{P}}{\lambda \mu c}, Gr = \frac{\rho_f \beta_{\bar{T}} g (T_1-T_0) d^2}{\mu c}, Br = \frac{(C_1-C_0) d^2 (\rho_p-\rho_f) g \beta_{\bar{C}}}{\mu c}, N_b = \frac{c \rho_p (C_1-C_0) D_B}{c \rho_f v}, N_t = \frac{D_T c \rho_p (T_1-T_0)}{T_m c \rho_f v}, B = \frac{A}{d} \end{aligned} \tag{9}$$

Where $Re, \delta, \omega, Gr, Pr, Br, \kappa, N_t, H, N_b$, and B represent the Reynold number, the dimensionless wave number, dimensionless concentration phenomena, the Grashof number, the Prandtl number, the Brinkman number, the porosity parameter, the Brownian motion number, the Hartman number, the thermophoresis parameter and the slip parameter, respectively.

Employing Eq. (9) in Eqs. (3)-(8) and applying the well-known physiological assumptions of low Renold number ($Re \ll 1$) and the long wavelength ($\delta \ll 1$) approximations in our present model, the governing equations can be simplified into dimensionless form as follows:

$$\frac{\partial u}{\partial x} + \frac{\partial v}{\partial y} = 0, \tag{10}$$

$$p_x = \frac{\partial s_{xy}}{\partial y} + Gr \theta + Br \omega - \left(H^2 + \frac{1}{\kappa} \right) (u + 1) \tag{11}$$

$$p_y = 0 \tag{12}$$

$$\theta_{yy} + Pr N_b \theta_y \omega_y + Pr N_t \theta_y^2 = 0, \tag{13}$$

$$N_b \omega_{yy} + N_t \theta_{yy} = 0, \tag{14}$$

Eq. (12) shows that the pressure field p is not the function of y , and by using this observation, we eliminate the gradient of pressure from Eq. (11) as below

$$\frac{\partial^2 s_{xy}}{\partial y^2} + Gr \theta_y + Br \omega_y - \left(H^2 + \frac{1}{\kappa} \right) u_y = 0 \tag{15}$$

Where s_{xy} is the dimensionless extra stress tensor and $s_{xy} = \frac{1}{1+\lambda_1} \frac{\partial u}{\partial y}$, (λ_1 is the Jeffery parameter)

However, the dimensionless form of corresponding physical boundary conditions is

$$u(h) = -1 - \frac{2\pi\epsilon\alpha\beta \cos(2\pi x)}{(1-2\pi\epsilon\alpha\beta \cos(2\pi x))} + \frac{B}{1+\lambda_1} \frac{\partial u}{\partial y}, \text{ and } (h) = \frac{2\pi\epsilon \sin(2\pi x)}{(1-2\pi\epsilon\alpha\beta \cos(2\pi x))}, \tag{16}$$

$$\theta = 1, \omega = 1 \text{ at } y = h = 1 + \epsilon \cos(2\pi x) \tag{17}$$

$$u = -1, u_y = 0, \theta_y = 0, \omega = 0 \text{ at } y = 0 \tag{18}$$

The Solution to the Problem

The closed-form solutions for the well-posed system of the differential equations for the velocity, the temperature and the concentration fields are achieved. Integrating Eqs. (13), (14) and (15) with respect to boundary conditions in Eqs.(16)-(18), the exact solution for the velocity profile $u(x, y)$, the temperature distribution $\theta(x, y)$ and the concentration profile $\omega(x, y)$ are obtained, respectively as follows:

$$u(x, y) = c_3 - \frac{(L_1L_2+L_3L_4+L_5-L_6)}{L_7L_8} \tag{19}$$

$$L_1 = e^{-My\sqrt{1+\lambda_1}}(-1 + e^{Pr(N_b+N_t)})hMc_1N_b(PrN_b + PrN_t - M\sqrt{1+\lambda_1}),$$

$$L_2 = (PrN_b + PrN_t + M\sqrt{1+\lambda_1})(PrN_b + PrN_t - hM\sqrt{1+\lambda_1})(PrN_b + PrN_t + hM\sqrt{1+\lambda_1}),$$

$$L_3 = e^{My\sqrt{1+\lambda_1}}(1 - e^{Pr(N_b+N_t)})hMc_2N_b(PrN_b + PrN_t - M\sqrt{1+\lambda_1}),$$

$$L_4 = (PrN_b + PrN_t + M\sqrt{1+\lambda_1})(PrN_b + PrN_t - hM\sqrt{1+\lambda_1})(PrN_b + PrN_t + hM\sqrt{1+\lambda_1}),$$

$$L_5 = e^{\frac{Pr(-h+y)(N_b+N_t)}{h}}Grh^3M^2N_b(1+\lambda_1)^{3/2}(-Pr^2N_b^2 - 2Pr^2N_bN_t - Pr^2N_t^2 + M^2(1+\lambda_1)),$$

$$L_6 = Bre^{-Pr(-h+y)(N_b+N_t)}hM^2N_t(1+\lambda_1)^{3/2}(-Pr^2N_b^2 - 2Pr^2N_bN_t - Pr^2N_t^2 + h^2M^2(1+\lambda_1)),$$

$$L_7 = ((-1 + e^{Pr(N_b+N_t)})hM^2N_b\sqrt{1+\lambda_1}(PrN_b + PrN_t - M\sqrt{1+\lambda_1})(PrN_b + PrN_t + M\sqrt{1+\lambda_1}),$$

$$L_8 = (PrN_b + PrN_t - hM\sqrt{1+\lambda_1})(PrN_b + PrN_t + hM\sqrt{1+\lambda_1}),$$

$$M = \left(H^2 + \frac{1}{\kappa}\right),$$

and

$$\theta(x, y) = -\frac{e^{(N_b+N_t)Pr}\left(-1+e^{-\frac{(N_b+N_t)Pr y}{h}}\right)}{\left(-1+e^{(N_b+N_t)Pr}\right)}, \tag{20}$$

$$\omega(x, y) = \frac{e^{(N_b+N_t)Pr(h-y)}hN_t-(N_b+N_t)y+e^{(N_b+N_t)Pr}(-hN_t+(N_b+N_t)y)}{\left(-1+e^{(N_b+N_t)Pr}\right)hN_b}, \tag{21}$$

In which the expressions for the parameters c_1 , c_2 , and c_3 are determined by applying the boundary conditions in Eq. (18).

To determine the expression for the stream function, we make use of the following relations

$$u = \frac{\partial \psi}{\partial y}, \tag{22}$$

Thus

$$\psi(x, y) =$$

$$\frac{-1}{2(-1+e^{Pr(N_b+N_t)})hM^2PrN_b(N_b+N_t)(1+\lambda_1)(PrN_b+PrN_t-M\sqrt{1+\lambda_1})(PrN_b+PrN_t+M\sqrt{1+\lambda_1})} \left(((-2c_3(-1 + e^{Pr(N_b+N_t)})hM^2PrN_b(N_b+N_t)(1+\lambda_1)(PrN_b + PrN_t - M\sqrt{1+\lambda_1})(PrN_b + PrN_t + M\sqrt{1+\lambda_1}) +$$

$$2e^{-\frac{\text{Pr}(-h+y)(N_b+N_t)}{h}} Gr h^4 M^2 N_b (1 + \lambda_1)^2 \left(Pr^2 N_b^2 + 2Pr^2 N_b N_t + Pr^2 N_t^2 - M^2 (1 + \lambda_1) \right) + \dots + C \quad (23)$$

Where C can be found by satisfying the boundary condition $\psi(h) = q$.

Graphical discussion

This part of the work is dedicated to analyzing the impacts of different flow physical parameters on graphic outcomes for the flow of MHD Jeffery nanofluid through cilia channel i.e. velocity distribution, temperature field, nanoparticle concentration, and trapping phenomena. The velocity profile attudes a parabolic trajectory with a maximum magnitude appearing in the middle part of the channel. The discussion is made for the fixed values $\{x = 0.01, \beta = 0.1, Br = 0.1, Pr = 0.7\}$ In Figure 2(a), the reduction influence of Hartman number H on the velocity profile $u(y)$ is recorded due to the normal effect of the magnetic field. This result is beneficial during surgery and critical operation to control redundant bleeding. However, we noticed an enhancement of $u(y)$ with increasing the permeability parameter κ i.e. more fluid passes through the pores via Figure 2(b). It is clear from Figure 2(c) that ascending values of the Grashof Gr number reduces the drag force, which, in turn, the axial velocity $u(y)$ will be accelerated. An increasing behavior for $u(y)$ exhibits due to the larger magnitude of Jeffery nanofluid parameter λ_1 , which is noted in Figure 3(a). The increasing effect of slip parameter B on the fluid velocity profile through Figure 3(b) is noted. The impact of the dimensionless eccentricity of ellipse parameter α on velocity distribution is demonstrated in Figure 3(c). We conclude that enhancement in α magnitude leads to stagnation of the largest amount of Jeffery fluid in the main stream of the flow field which induces mitigation in its velocity. Figures 4(a) and (b) recorded the dissimilar behavior for the velocity profile as the Brownian motion number N_b and the thermophoresis parameter N_t increase. Whereas two opposite reactions upon velocity profile are seen via increment the dimensionless magnitude of the cilia length ϵ i.e. decay in $u(y)$ magnitude is noticed for the region $(0.2 \leq y \leq 0.7)$ and after this region the velocity value continues to rise along the channel, see Figure 4(c).

The graphs in Figures 5 (a),(b), and (c) inspect the behavior of temperature profile under the effect of the Prandtl number Pr , Brownian motion number N_t , and dimensionless magnitude of the cilia length ϵ , respectively. It can be observed from these figures that the temperature profile exhibits a parabolic nature. Moreover, it is admitted from the plots that $\theta(y)$ exactly grows in the same manner with increasing the values of Pr , and N_t . Whereas a decay in temperature profile is noticed with ascending values of ϵ parameter. The evolution in nanoparticle concentration distribution via ascending of embedded parameters Pr , N_t , and N_b respectively illustrates in Figure 6. Diminishing behavior for the three selected parameters on $\omega(y)$ curve can be revealed in Figures 6(a) and (b), respectively. However $\omega(y)$ is very sensitive against to any small rises in N_b value see Figure 6(c). In our study the graphical observation of the discussed profiles for $\theta(y)$ and $\omega(y)$ are in complete agreement with those illustrated in Imran et al. [10] study.

The configuration of the heat transfer coefficient $\left(Z(x) = \frac{\partial h}{\partial x} \times \theta_y |_{y=h} \right)$ versus the x -axis is inspected under the impact of the following involved physical parameters Prandtl number Pr , Brownian motion number N_t , and thermophoresis parameter N_b through Figures 7(a)-(c). It can be revealed. One can notice from these figures the oscillatory behavior for the heat transfer coefficient due to peristaltic walls. Furthermore; $Z(x)$ is an increasing function of increasing the three mentioned parameters i.e. Pr , N_t and N_b at other points and decreasing at other points successively and continually along the channel wall.

In human body channels especially the esophagus conduits which contains within cilia tips create metachronal wave motion which causes a trapping phenomenon (formation of an enclosed bolus of the fluid particles entirely surrounded by fluid streamlines) in return moves along the channel with metachronal wave speed. In this part of the discussion, we will examine the influence of physically interesting parameters on fluid streamlines by sketching the stream function against various values of the Hartman number H , the porosity parameter κ , the Grashof number Gr , α the elliptical motion eccentricity dimensionless value, Jeffery parameter λ_1 , Brinkman number Br , the Brownian motion number N_t and the dimensionless magnitude of the cilia length ϵ respectively. From these figures, we noticed that the generating two separated trapping boluses in the central part of the channel. Figure 8 depicts a diminishing in size and number of the trapped bolus in which the two boluses are connected into one big bolus in the center of the channel via increasing the value of H . However; the impact of κ on streamlines is illustrated in Figure 9. It is evident from the figure that the size of trapping bolus enhances and more streamlines surrounded the boluses. Figures 10, 11 and 12 show the shrinking effect for Gr , α and λ_1 on trapping bolus size and fewer numbers of bolus recognized especially with α larger value. The shape of the trapped bolus deforms and decreases for larger values of Br see Figure 13. It reveals from Figure 14 that the volume of the trapping bolus tends to enlarge as N_t increases furthermore, the two boluses are merged together and become a single bolus in the central part of the channel. A remarkable effect of ϵ on streamlines from Figure 15 is illustrated. When the value of $\epsilon = 0.1$, the trapped bolus disappeared and the flow turned into straight streamlines while the bolus is generated and increased for $\epsilon > 0.1$.

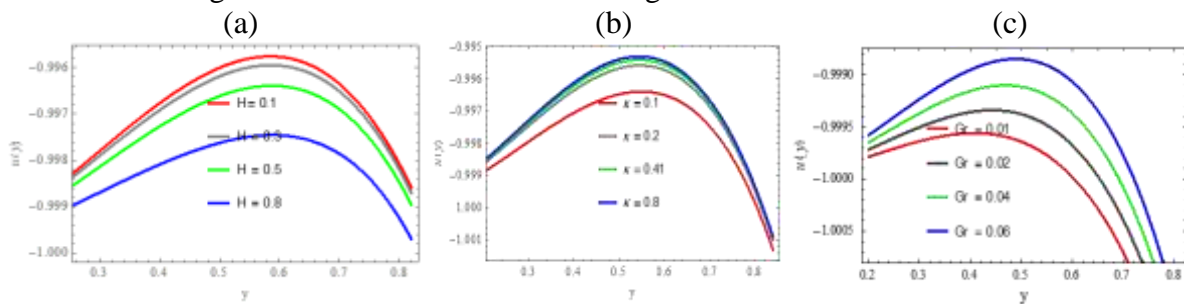


Figure 2: Velocity profile against ascending values of (a) Hartman number H (b) Porosity parameter κ (c) Grashof number Gr .

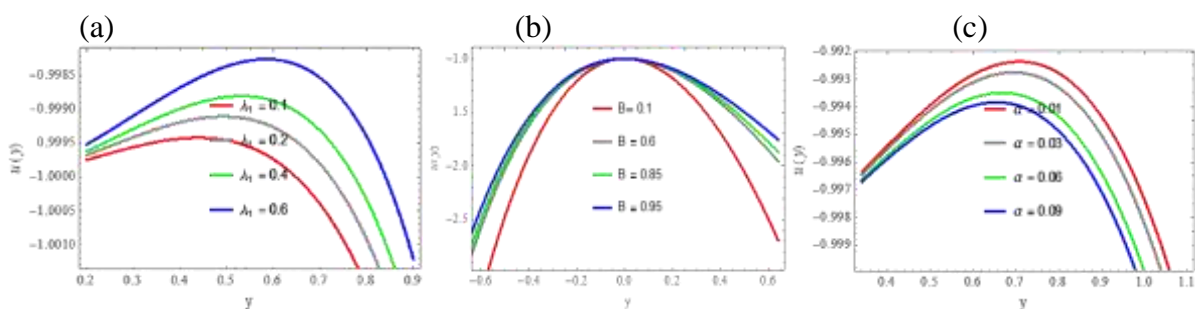


Figure 3: Velocity profile against ascending values of (a) Jeffery parameter λ_1 (b) slip parameter B (c) dimensionless eccentricity of ellipse parameter α .

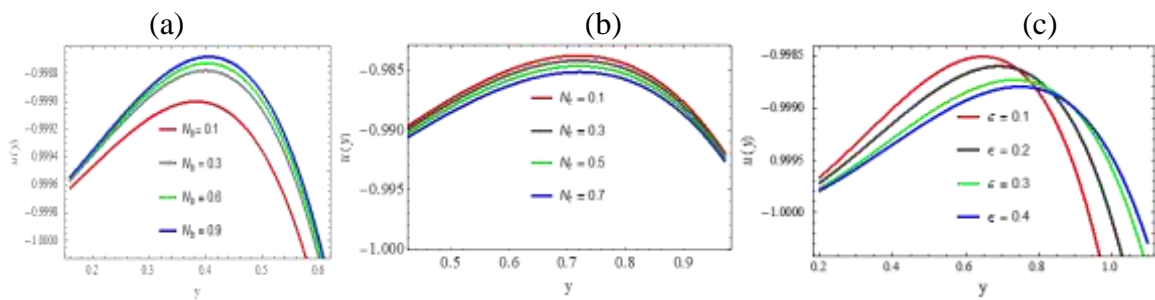


Figure 4: Velocity profile against ascending values of (a) thermophoresis parameter N_b (b) Brownian motion number N_t (c) dimensionless magnitude of the cilia length ϵ .

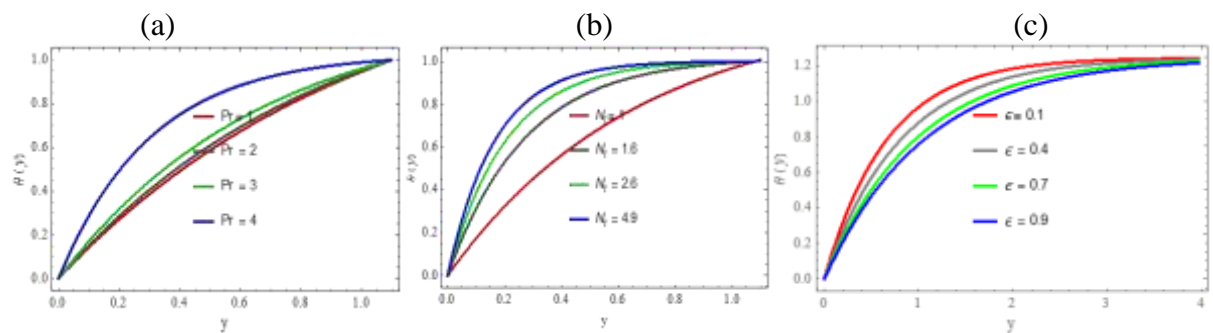


Figure -5 Temperature profile $\theta(y)$ for ascending values of (a) Prandtl number Pr (b) Brownian motion number N_t (c) dimensionless magnitude of the cilia length ϵ .

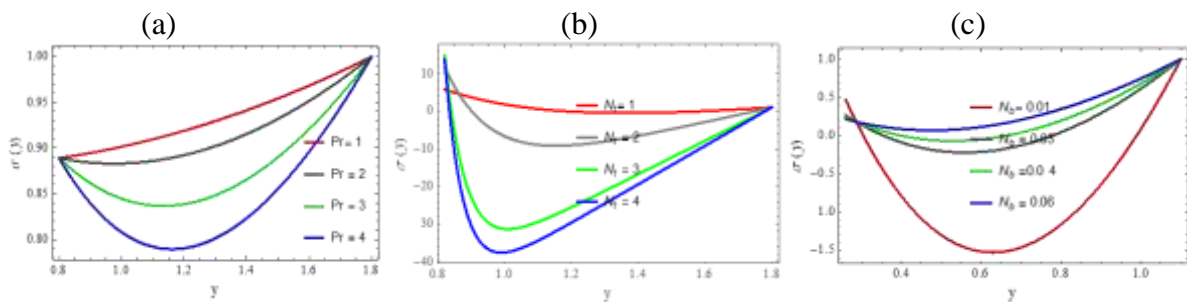


Figure 6: Nanoparticle concentration profile $\omega(y)$ for ascending values of (a) Prandtl number Pr (b) Brownian motion number N_t (c) thermophoresis parameter N_b .

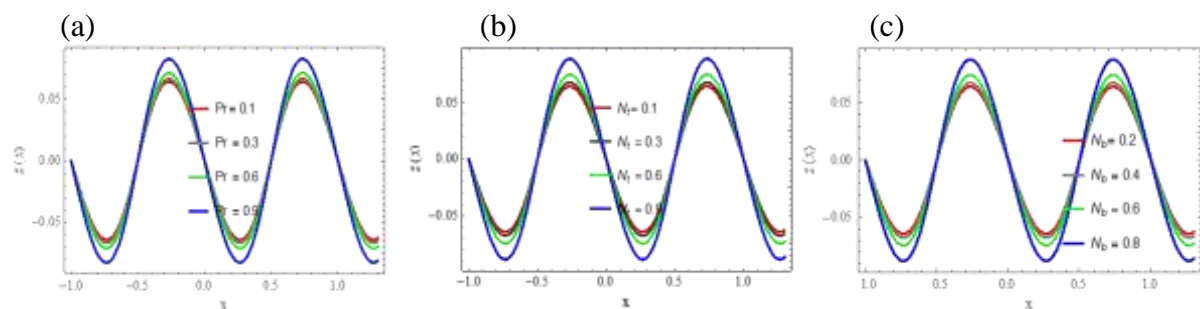


Figure 7: Heat transfer profile $Z(x)$ for ascending values of (a) Prandtl number Pr (b) Brownian motion number N_t (c) thermophoresis parameter N_b .

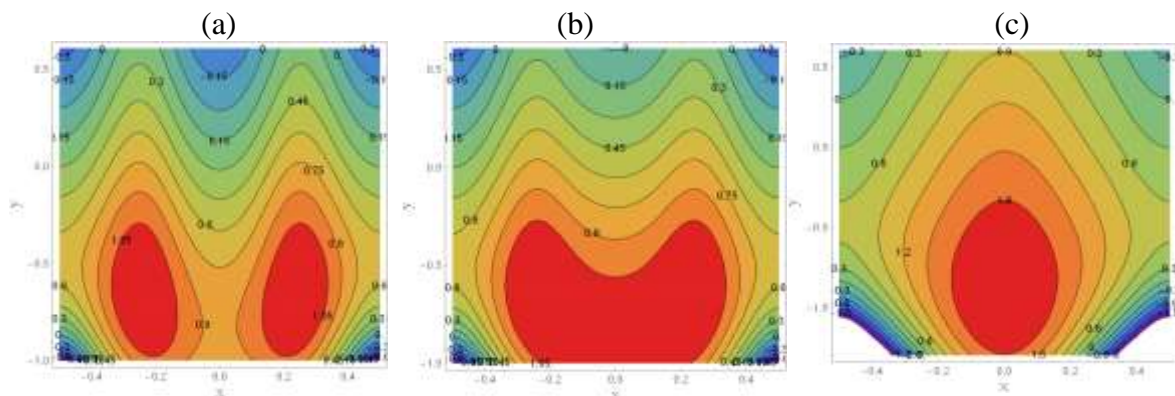


Figure 8: Streamlines for ascending values of Hartman number (a) $H = 0.8$ (b) $H = 0.9$ (c) = 1.4 .

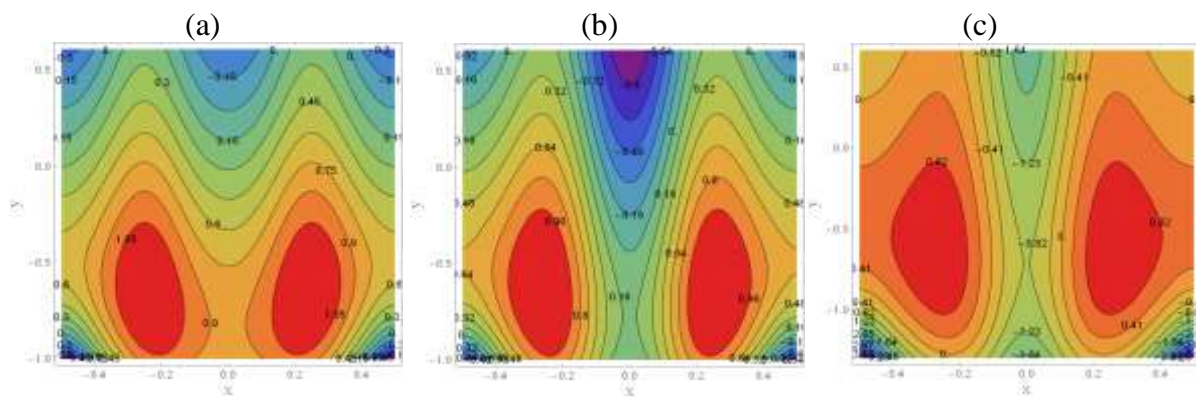


Figure 9: Streamlines for ascending values of porosity parameter (a) $\kappa = 0.8$ (b) $\kappa = 0.9$ (c) = 1.4 .

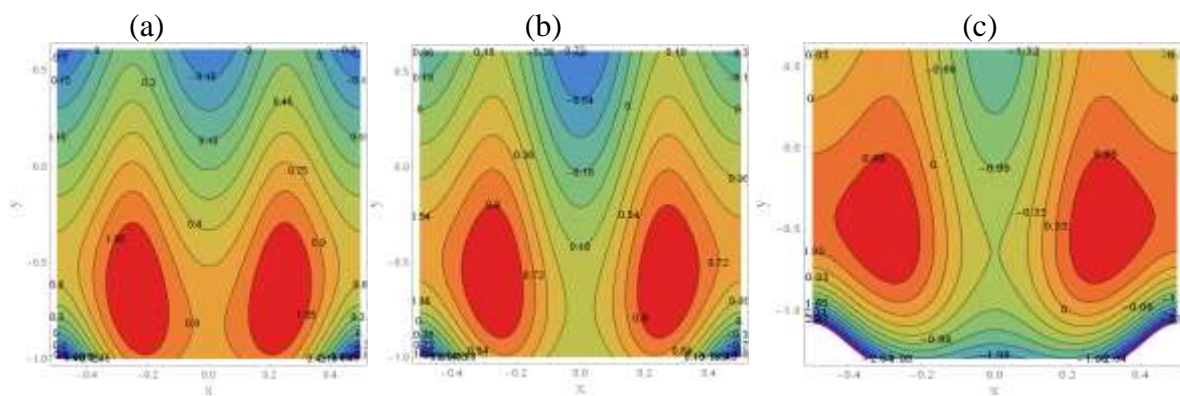


Figure 10: Streamlines for ascending values of Grashof number (a) $Gr = 0.8$ (b) $Gr = 1.2$ (c) = 1.9 .

(a)

(b)

(c)

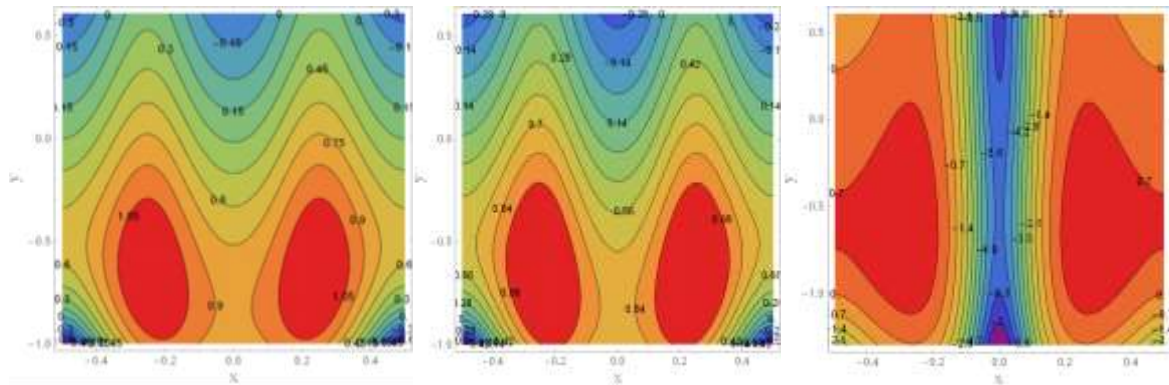


Figure 11: Streamlines for ascending values of elliptical motion eccentricity dimensionless value (a) $\alpha = 0.03$ (b) $\alpha = 0.08$ (c) $\alpha = 0.3$

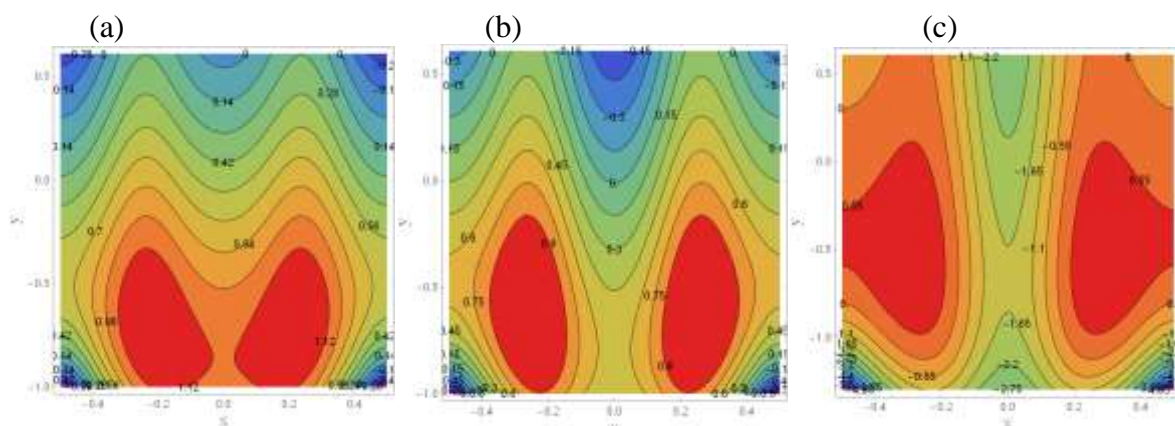


Figure 12: Streamlines for ascending values of Jeffery parameter (a) $\lambda_1 = 0.7$ (b) $\lambda_1 = 0.9$ (c) $\lambda_1 = 1.2$

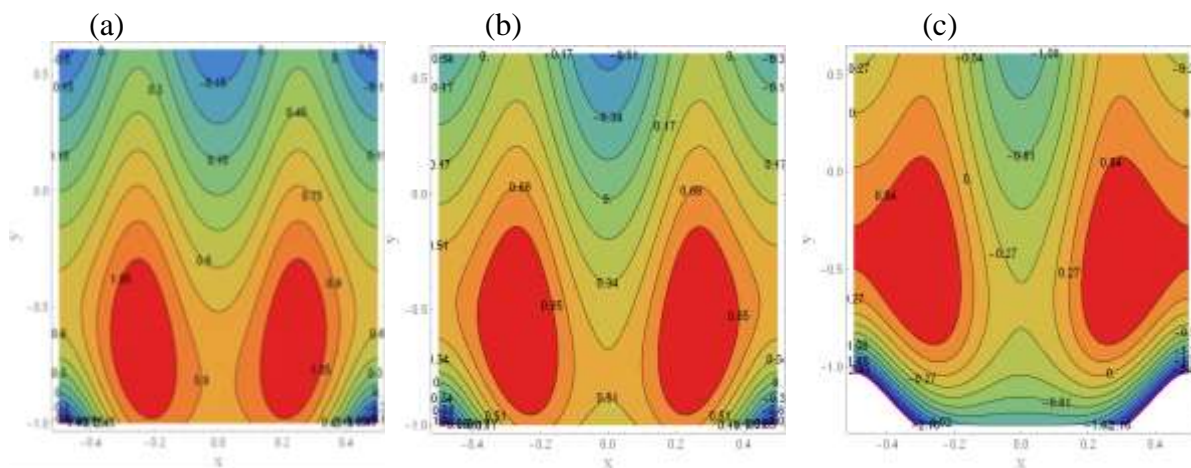


Figure 13: Streamlines for ascending values of Brinkman number (a) $Br = 0.7$ (b) $Br = 0.9$ (c) $Br = 1.2$

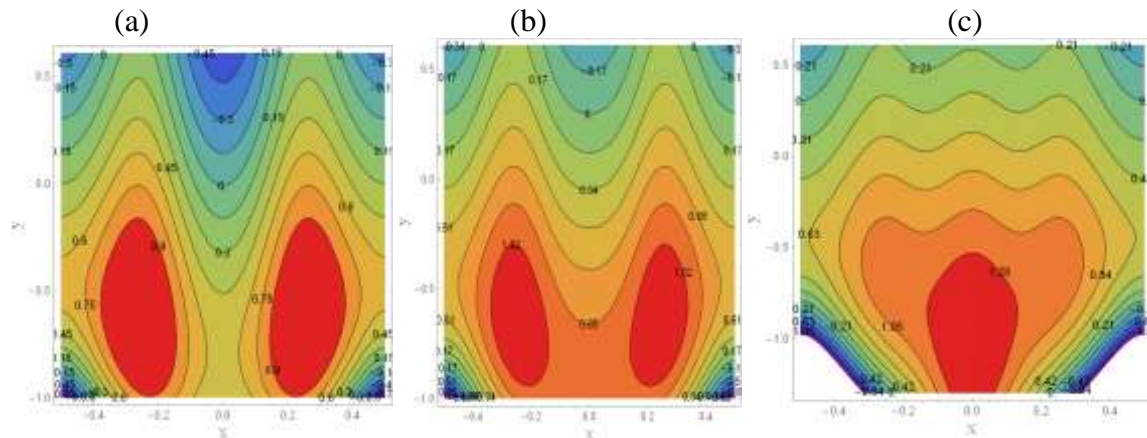


Figure 14: Streamlines for ascending values of Brownian motion number (a) $N_t = 0.03$ (b) $N_t = 0.05$ (c) $N_t = 0.08$

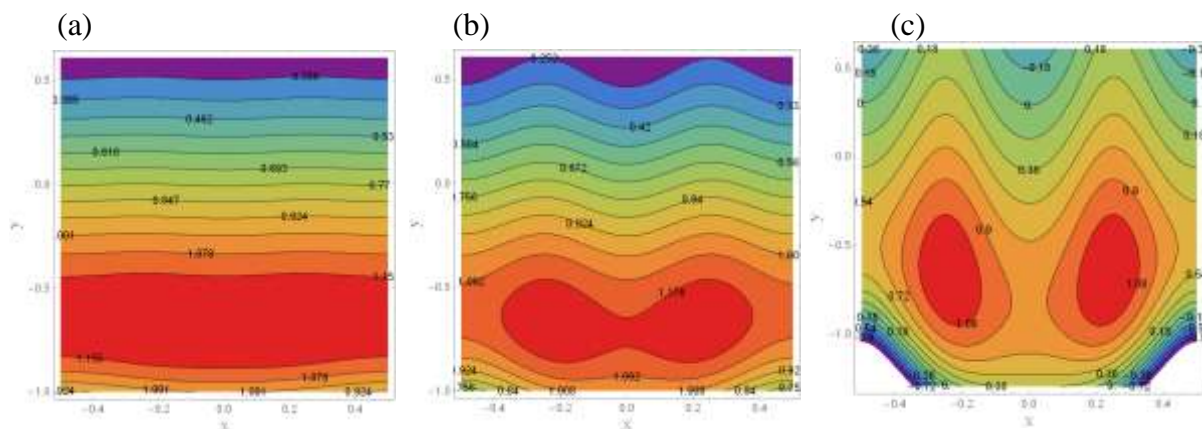


Figure -15 Streamlines for ascending values of cilia length parameter (a) $\epsilon = 0.1$ (b) $\epsilon = 0.3$ (c) $\epsilon = 0.8$

Conclusion

This article analyzes the metachronal waves of the Jeffery nanofluid propagate due to flow through ciliated channel filled with porous media. The mathematical equations that govern the flow were formulated and simplified depending on the assumption of long wavelength and small Reynolds number. The reduced partial differential equations associated with slip boundaries are exactly solved by the Mathematica program. The results are discussed through figures and bellows some important outcomes are listed.

1. The velocity profile is an increasing function via mounting the parameters κ, Gr, λ_1, B and N_b whereas it is a decreasing function with H, α and N_t .
2. It is observed that the velocity profile first diminishes and then enhances with increasing ϵ value.
3. The parameters Pr and N_t exhibit risen effect on temperature distribution $\theta(x, y)$. However, they exhibit opposite consequences on nanoparticle concentration $\omega(x, y)$.
4. Dimensionless magnitude of the cilia length ϵ causes retardation in $\theta(x, y)$.
5. An oscillatory behavior is witnessed of the heat transfer coefficient $Z(x)$ magnitude upon variation of Pr, N_t , and N_b parameters.

6. The trapping bolus revealed a reversed behavior with increments of H , Br , λ_1 , Gr , α and N_t values whereas direct effect to κ on the trapped bolus in size and number is recorded.

7. Remarkable effect of ϵ on streamlines depicted, for a certain value ($\epsilon = 0.1$), the flow presents The flow is straight lines and free of the trapped bolus, while we notice the appearance of the bolus phenomenon for ϵ values higher than that.

8. It is worth to mentioning that our work considered an extension of the study given by Imran et al. [10], they investigated the effect of ciliary channel on the nanofluid flow, while here, we extended the research to explore the effect of the ciliary channel, porous medium and normal magnetic field on Jeffery nanofluid flow.

References

- [1] R. E. Abo-Elkhair, K. S. Mekheimer and A. A. Moawad, "Cilia walls influence on peristaltically induced motion of magneto-fluid through a porous medium at moderate Reynolds number," *Journal of The Egyptian Mathematical Society*, vol. 25, no. 2, pp. 238-251, 2017.
- [2] S. Anber, . Q. Aleesha and . N. Sohail, "[2] Anber Saleem, Aleesha Qaiser and Sohail Nadeem, 2Physiological flow of biomedical compressible fluids inside a ciliated symmetric channel," [2] Anber Saleem, Aleesha Qaiser and Sohail Nadeem, 2020, "Physiological flow of bio Journal of Advances in Mechanical Engineering, vol. 12, no. 7, p. 1–11., 2020.
- [3] . K. Azeem, . G. Abuzar, . W. Muhammad, G. Abuzar and A. K. Waqar, "Cilia-driven fluid flow in a curved channel : Effects of complex wave and porous medium," *Journal of Fluid Dynamics Research*, vol. 52, no. 1, 2020.
- [4] M. Sleight, *The Biology of Cilia and Flagella*, New York : MacMillan , 1962.
- [5] M. C.E., " C. E. Miller An investigation of the movement of Newtonian liquids initiated and sustained by the oscillation of mechanical cilia," in *Aspen Emphysema*, 1967.
- [6] . K. jmn S.N. and . O. P.R. , "jmn S.N. Khaderi, Fluid structure interaction of three dimensional magnetic artificial cilia," *Fluid Mechanics*, vol. 708, no. 2012, p. 303 – 328. , 2012.
- [7] . F. A. A. , . S. Zahir, . S. Meshal, . B. Ebenezer and . R. Prosun, "Axisymmetric mixed convective propulsion of a non-Newtonian fluid through a ciliated tubule," in *AIP Advances*, 2020.
- [8] Noreen Sher Akbar and Adil Wahid Butt , "Bio mathematical venture for the metallic nanoparticles due to ciliary motion," *Computer Methods and Programs in Biomedicine*, vol. 134, pp. 43-51, 2016.
- [9] . K. Ramesh, D. Tripathi and Anwar Bég.O., "Cilia-assisted hydromagnetic pumping of biorheological couple stress fluids," *Propulsion and Power Research*, vol. 8, no. 3, pp. 221-233, 2019.
- [10] Ali Imran, Rizwan Akhtar, Zhu. Zhiyu, Muhammad Shoaib and Muhammad Asif Zahoor Raja, "Heat transfer analysis of biological nanofluid flow through ductus efferentes," in *AIP Advances*, 2020.
- [11] S. U. S. Choi, Enhancing thermal conductivity of fluids with nanoparticles. in *Developments and Applications of Non-Newtonian fluid*, New York, NY, USA: [1] S. U. S. Choi, 1995, "Enhancing thermal conductivity of fluids with nanoparticles Ows, D. A. Siginer and H. P. Wang, Eds., 1995.
- [12] Khalid Nowar, "Peristaltic Flow of a Nanofluid under," *Hindawi Publishing Corporation, Mathematical Problems in Engineering*, vol. 2014, 2014.
- [13] Aysha Rehman, Azad Hussain and Sohail Nadeem, "Assisting and Opposing Stagnation Point Pseudoplastic Nano Liquid Flow towards a Flexible Riga Sheet," *Mathematical Problem in Engineering, Hindawi*, vol. 2021, p. 14 pages, 2021.
- [14] Aamir Ali, Y. Ali, D. N. Khan Marwat and M. Awais, Z., "Peristaltic flow of nanofluid in a deformable channel with double diffusion," *Springer Nature Applied Sciences*, 2019.

- [15] Safia Akram, M. Zafar and S. Nadeem, "Peristaltic transport of a Jeffrey fluid with double-diffusive convection in nanofluids in the presence of inclined magnetic field," *International Journal of Geometric Methods in Modern Physics*, vol. 15, no. 11, p. 21 pages, 2018.
- [16] Saba S. Hasen and Ahmed M. Abdulhadi, "MHD Effect on Peristaltic Transport for Rabinowitsch Fluid through A Porous Medium in Cilia Channel," *Iraqi Journal of Science*, vol. 61, no. 6, pp. 1461-1472, 2020.
- [17] Mohammed R. Salman and Hayat A. Ali, "Approximate Treatment for The MHD Peristaltic Transport of Jeffrey Fluid in Inclined Tapered Asymmetric Channel with Effects of Heat Transfer and Porous Medium," *Iraqi Journal of Science*, vol. 61, no. 12, pp. 3342-3354, 2020.